Exogenous brain stimulation pulses are carried along the motor pathways from pallidum to distant targets: Results of a transfer function analysis

Maral Kasiri[1], Jessica Vidmark[1], Estefania Hernandez-Martin[2], S. Alireza Seyyed Mousavi[2], and Terence D. Sanger[1,2,3]

[1] Department of Biomedical Engineering, University of California-Irvine, Irvine, CA, USA
kasirim@uci.edu
[2] Department of Electrical Engineering and Computer Science, University of California-Irvine, Irvine, CA, USA
[3] Department of Neurology, Children's Health Orange County, Orange, CA, USA

Abstract. Deep brain stimulation (DBS) is a neuromodulation method for treatment of various neurological disorders. It is often assumed that the primary effect of DBS occurs at the site of stimulation, similar to the effects of lesions. However, recent work has shown that DBS can lead to robust evoked potentials (EP) not only at the stimulation site, but also in multiple distant brain regions. While the significance of these EPs for therapeutic outcomes is not known, it appears that the electrical effects of DBS have at least a partial modulatory impact on downstream targets. Nonetheless, it remains unclear how DBS pulses travel to the distant targets. The possible scenarios include, but are not limited to, orthodromic or antidromic pathways, accessory pathways, normally inhibited pathways, and direct electromagnetic activation of distant sites. The ability to record signals from brain regions with DBS on and off provides an opportunity to determine the mechanism of DBS. This study aims to examine how electrical stimulation from DBS pulses is carried along neural pathways. We hypothesize that the pathways that transmit DBS pulses include the pathways that transmit endogenous neural signals, and are more likely to travel in the same direction as endogenous signals. To test this hypothesis, we performed a transfer function analysis on deep brain recordings when DBS is on and off to compare the transmission of signals from electrical stimulation with the transmission of endogenous signals. Our results support our claim that the electrical pulses travel at least in part along the normal motor pathways.

Keywords: Deep brain stimulation · Empirical transfer function · Signal transmission · Movement disorder · DBS mechanism

1 Introduction

Dystonia is a movement disorder characterized by involuntary and repetitive muscle contractions, resulting in abnormal posture and movements [1]. In cases that medication and other medical interventions do not improve the dystonic symptoms, DBS is an alternative symptomatic treatment [1–4]. DBS is a neuromodulation method that involves implantation of depth electrodes at potential targets in the brain, through which electrical pulses are transmitted to modulate neuronal activity [5], potentially by interrupting or distorting endogenous abnormal activity. Despite recent advancements in clinical applications of DBS, its underlying mechanism is not well understood [1, 6–9].

Identifying the DBS signal pathways is essential for computational modeling and direct measurement of the effects of DBS on brain networks [10]. While anatomic evidence from noninvasive technologies such as diffusion tensor imaging (DTI) is available, this provides only indirect support for anatomical connectivity and is not sufficient for assessing the magnitude and delay of signal transmission and functional connectivity [11]. Direct measurement is required to learn about the signal transmission along these pathways. Furthermore, evidence for the presence of a pathway and the presence of signal correlations at either end of that pathway is not sufficient to establish causality or the direction of signal transmission.

One way to definitively map neural transmission in deep brain networks is to insert an exogenous stimulation signal and measure its effect on distant targets [12]. However, exogenous signals can travel from the source to the target through many pathways, including "normal" (orthodromic) pathways, antidromic pathways, accessory pathways that would not normally be active, and direct electromagnetic activation of distant sites [7]. Alternative mechanisms also include activation of pathways that are normally inhibited or those with high threshold or those that are not accessible to stimulation, including polysynaptic pathways. Electrical stimulation is an un-natural and non-physiological input to the brain. It non-selectively activates and depolarizes wide group of neurons that would be much more selectively activated in physiology.

To distinguish these possibilities, we compare the transmission of DBS stimulation signals to a transfer function representation of endogenous signals, at two ends of an known anatomical pathway. Note that the estimated transfer function does not indicate causality, because transfer functions are bi-directional in nature and the causation flow is not clear [13, 14]. Nevertheless, we can set the input and output of the system based on the evidence of physiological connections [15] and extract useful information based on those presumptions. The study methodology was designed to test our hypotheses that the pathways that transmit external electrical stimulation (exogenous signals, DBS) include the pathways that transmit intrinsic neural signals (endogenous signals).

To test our hypotheses, we made use of intracranial brain signals (local field potentials; LFPs) recorded from seven subjects as part of their clinical evaluation for implantation of permanent DBS electrodes.Stereoelectroencephalography (sEEG) leads were implanted into potential DBS targets followed by one week of exten-

sive tests and recordings in an inpatient neuromodulation unit (NMU) with the clinical goal of finding the ideal target region(s) for each patient's permanent DBS lead(s) [3]. Clinical evaluation focused on capturing evoked responses in ventralis oralis anterior/posterior (VO) and ventral anterior (VA) subnuclei of thalamus, and subthalamic nucleus (STN) during stimulation in globus pallidus internus (GPi), as well as the responses in GPi due to stimulations in VO, VA, and STN. Clinical data also included recordings of the natural LFP oscillations during a voluntary reaching task, while stimulation was off. If a significant fraction of the variance of the evoked response from the exogenous signal can be explained by a transfer function computed using the endogenous signals, we can claim that exogenous signals travel primarily by the physiologically used endogenous pathways. Additionally, we hypothesize that the fraction of variance in EP explained by the response of the estimated transfer function is significantly higher in the orthodromic direction than in the antidromic direction. This further supports our hypothesis that the stimulation pulses are primarily transmitted by a mechanism similar to that of endogenous signals.

2 Materials and methods

2.1 Patient selection

Patients with dystonia (acquired, genetic, or neurometabolic) were selected for DBS surgery if there existed potential stimulation target(s) identifiable with magnetic resonance imaging (MRI) and if alternative medical therapies had been ineffective [16]. The patients were diagnosed with dystonia by a pediatric movement disorder specialist (T.D.S.) using standard criteria [17]. The patients' demographics are described in Table 1. Patients or parents of minor patients provided Health Insurance Portability and Accountability Act (HIPAA) authorization for the research use of protected health information and written informed consent for surgical procedures conforming to standard hospital practice, and for research use of electrophysiological data before the procedure. The research use of data was approved by the institutional review board of Children's Health Orange County (CHOC). All the surgical procedures and experiments took place at CHOC.

2.2 Data acquisition

Up to 12 temporary sEEG AdTech MM16C depth leads (AdTech Medical Instrument Corp., Oak Creek, WI, USA) were implanted into potential DBS targets. Based on prior studies of clinical efficacy in children with dystonia , typical target regions for DBS include STN and GPi in basal ganglia, ventral intermediate (VIM), VO, and VA thalamic subnuclei [3]. The position of leads and electrode contacts was determined by alignment of a post-operative computed tomography (CT) scan with the preoperative MRI anatomic scan [19, 20]. Each implanted lead contains 6 low-impedance (1–2 $k\Omega$) ring macro-contacts with 2 mm height

Table 1: Patient demographics. All participants are male, 8-25 years old. ✓: EP from GPi stimulation exists; ×: EP was not observed. GA1: Glutaric Aciduria type 1. CP: Cerebral Palsy.

Subject	Characteristic	VO	VA	STN
S1	CP; Hyperkinetic dystonia	✓	✓	✓
S2	Mitochondrial disease; Hypertonic dystonia, dyskinesias	✓	✓	✓
S3	Mitochondrial disease; Hypertonic and hyperkinetic dystonia	✓	×	✓
S4	Unknown; Tremor, Ataxia; hyperkinetic dystonia	✓	×	✓
S5	KMT2B [18]; Chorea, hyperkinetic dystonia	✓	✓	✓
S6	CP; Tremor, hyperkinetic dystonia	✓	✓	✓
S7	GA1; Hypertonic and hyperkinetic dystonia	✓	✓	✓

and 5 mm on-center spacing, as well as 10 high-impedance (70–90 $k\Omega$) microwire electrodes (50-µm diameter) referred to as micro-contacts. The micro-contacts are arranged in groups of 2 or 3, evenly spaced around the circumference of the lead shaft, halfway between neighboring pairs of macro-contacts. The leads were connected to Adtech Cabrio™ connectors that included a custom unity-gain preamplifier for each micro-contact to reduce noise and motion artifacts. Macro-contacts bypassed the preamplifiers to allow for external electrical stimulation. This setup enables clinicians to stimulate through macro-contacts while recording through all other contacts. All data used in this study were recorded through micro-contacts and sampled at 24 kHz by a system with a PZ5M 256-channel digitizer and RZ2 processor, and stored in a RS4 high speed data storage (Tucker-Davis Technologies Inc., Alachua, FL, USA). Brain activity was recorded within 24 to 96 hours after surgery in two modes: 1) while the stimulation was off, and the patient was performing a voluntary reaching task with the upper limb contralateral to LFP recordings (endogenous signals). (Figure 1a) 2) while the patient was at rest and unilateral stimulation was on. Approximately 1200 DBS pulses (exogenous signals) were administered through two adjacent macro-contacts (anode and cathode) at a time, with 90-µs bandwidth and 3-V voltage at 25 Hz, eliciting DBS evoked potentials [EPs] (Figure 1b). In order to reduce the stimulation artifacts, we stimulated through each contact pair in two trials, with the cathode and anode switched. When the resulting signals are added, the opposite artifact polarities cancel out while the evoked response polarity is augmented. The experimental protocol, movement-LFP synchronization, and the stimualtion protocol are detailed in our previously published works, Kasiri et al. [4], Hernandez-Martin et al. [20], and Vidmark, Hernandez-Martin, and Sanger [16]. In order to primarily evaluate responses to monosynaptic transmission, we used recordings from GPi, VO, VA, and STN, as illustrated in Figure 1.

2.3 Data analysis

In order to determine whether exogenous signals travel via the same pathways that carry endogenous brain signals, we compared the DBS EPs with the im-

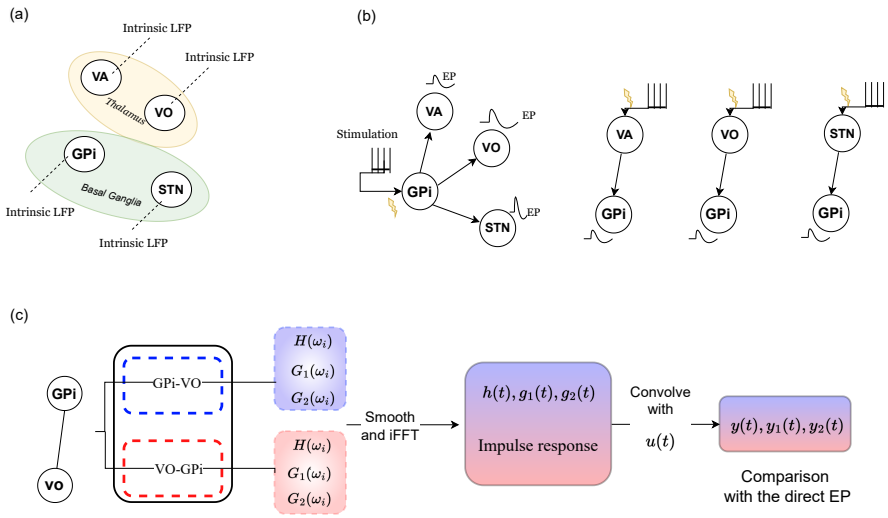

Fig. 1: a) Schematic of all recording targets when stimulation is off. b) Schematic of all recording and stimulation targets when stimulation is administered in one target, separately. c) Highlights the pipeline of transfer functions computations and comparisons for one pathway connecting the GPi and VO electrodes. Note that GPi to VO is orthodromic and VO to GPi is antidromic and we computed three transfer functions, $H(\omega_i)$, $G_1(\omega_i)$, and $G_2(\omega_i)$, for each direction and performed pairwise comparison between their responses, $y(t)$, $y_1(t)$, and $y_2(t)$.

pulse response of a system defined between the same two points in the brain. In other words, we compared the response at a distant region elicited by DBS at the stimulation site with the impulse response of a transfer function between the distant and stimulation sites in the absence of DBS. Transfer functions are specified in the frequency domain, while evoked potentials are specified in the time domain; therefore, we inter-converted the time and frequency domains using Fourier transform analysis and performed comparisons in time domain [21]. The method pipeline is depicted in Figure 1c. All data analysis was performed in MATLAB R2021a (The MathWorks, Inc., Natick, MA, USA).

Endogenous signals transfer function computation. The endogenous LFPs were notch filtered at 60 Hz and high-pass filtered at 1 Hz, to remove drift, and split into ∼50 two-second segments. We computed the empirical transfer function estimate (ETFE), $H(\omega_i)$, from the stimulation site (input) to the respective distant target (output), for each 2 seconds segment of recordings (See Figure 2 for a schematic representation of the system). Therefore, $H(\omega_i)$ is given by

$$H(\omega_i) = \frac{Y(\omega_i)}{U(\omega_i)} \tag{1}$$

where $Y(\omega_i)$ is the Fourier transform of the output signal and $U(\omega_i)$ is the Fourier transform of the input signal at frequency ω_i and $H(\omega_i)$ is the transfer function at that frequency [21]. This transfer function is a complex number that indicates the gain (signal amplification) and the phase shift from the input to the output for each frequency [21].

Exogenous signals transfer function computation. The micro-electrode recordings during DBS were notch filtered (at 60 Hz, including five harmonics) and high-pass filtered at 1 Hz and split into 11-ms segments starting from 1 ms prior to stimulus onset (stimulus artifact). After upsampling the recordings, stimulus artifacts were located using the 'findpeaks' function in MATLAB. Outlier segments were labeled and removed from the data if the artifact amplitude was not within their ± 3 standard deviations. All the remaining segments were subsequently aligned through cross-correlation of time-0 artifacts. This resulted in approximately 1000 segments per stimulus location, which were finally averaged to increase signal-to-noise ratio [22]. The stimulus-triggered averaging methodology presented by Sinclair et al. [22] was repeated for both sets of polarity reversed stimulation settings, which were finally aligned to produce a polarity-reversed average with smaller stimulus and decay artifacts [16, 19].

Using the DBS EPs, we computed two additional transfer functions to investigate whether the target EP results directly from the DBS signal, or from transmission of local responses of neural tissue near the stimulating electrode. The first case would correspond to DBS depolarization of nearby efferent axons, while the second case would correspond to DBS depolarization of nearby neural cell bodies, with subsequent propagation of neural signal. Therefore, we considered these two cases, in which (a) G_1 is a transfer function with the stimulation itself as the system input, and (b) G_2 is a transfer function with the stimulation-site DBS EP as its input. In both cases, the output is considered to be the distant target's EP. See Fig. 3 for a schematic model of these two cases.

It is worth noting that although the window sizes for DBS EP and endogenous LFP signals differ (10 ms versus 2 s), this disparity does not influence the final results. The EP window size is a mere 10 ms but represents an average of 1000 segments, resulting in enhanced signal smoothness and it is only used for confirmation of the efficacy of the off-stim ETFEs. We selected a window size of 2 seconds for the endogenous LFP to achieve higher frequency domain resolution and greater clarity when calculating the impulse responses and ETFEs. We then compared the EPs and impulse responses solely for the duration of the response, which is 5ms.

Nonetheless, the computed spectral estimates of the endogenous signals transfer functions alter drastically in higher frequencies because the ETFE variance does not diminish with large numbers of samples (Figure 4 top). Therefore, we utilized a smoothing method to smooth out the ETFE [14, 23].

Transfer function smoothing. We used local linear kernel smoothing regression to smooth the ETFEs in the frequency domain by solving a weighted

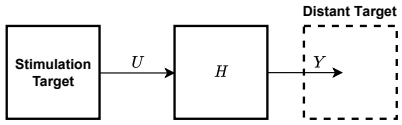

Fig. 2: endogenous signal pathway system schematic, where one end of the pathways is the system input and the other end is the system output.

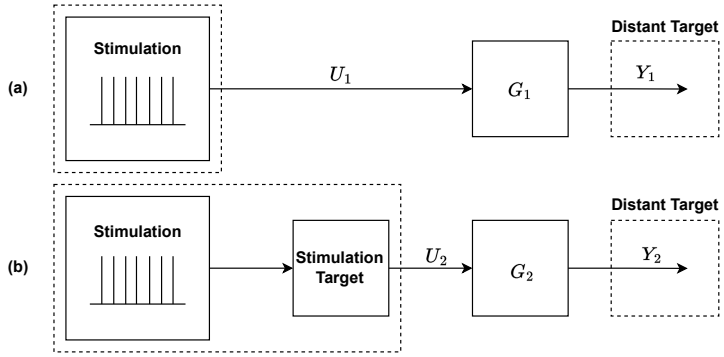

Fig. 3: Schematic for the system transfer function of DBS EPs: a) Direct stimulation of efferent axons by DBS stimulation.; and b) Stimulation of local neurons by DBS, with propagation of the subsequent signal to the target. In case (a), we expect the shape of the DBS signal to be the best predictor of the target response. In case (b), we expect the shape of the local EP at the stimulation site to be the best predictor of the target response.

least-squares (WLS) problem. The local linear estimator can be obtained by [14, 23–25]:

$$H(\omega_0) = \frac{1}{N} \frac{\sum_{i=1}^{N} (S_2 - (\omega_0 - \omega_i)^T S_1) K(\frac{\omega_0 - \omega_i}{h}) H(\omega_i)}{S_2 S_0 - S_1^2}, \tag{2}$$

where $H(\omega_0)$ is the smoothed transfer function, $K(\frac{\omega_0-\omega_i}{h})$ is the Gaussian kernel function, $K(z) = exp(-\frac{z^2}{\sqrt{2\pi}})$, with the bandwidth of $b = 50Hz$, and S_i is given by:

$$S_i = \frac{1}{N} \sum_{i=1}^{N} (\omega_0 - \omega_i)^i K(\frac{\omega_0 - \omega_i}{b}). \tag{3}$$

The resulting ETFE serves as an asymptotically unbiased estimator of the frequency response function [14]. Figure 4 shows an example of Bode magnitude plot of the estimated and the smoothed endogenous signals' transfer function (top) and the DBS EPs transfer function (bottom).

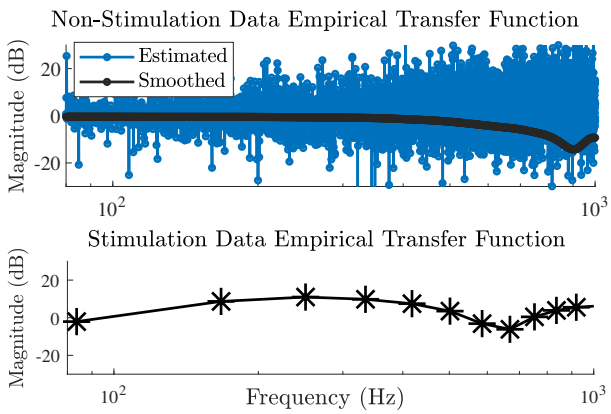

Fig. 4: (Top) Bode magnitude plot of a raw and smoothed ETFE from the endogenous signal recordings. (Bottom) Bode magnitude of a stimulation evoked potential transfer function. Note that the smoothing method has no effect on the stimulation evoked potential transfer function, as the response duration is brief (∼5 ms) and not well resolved in the frequency domain; confirming that the smoothing method does not introduce distortions to the system.

Simulation and comparison method. Let $u(t)$ be a pulse with similar specification to the true stimulation (90-μs pulse width and 3-V amplitude). Let $h(t)$ be the inverse Fourier transform (iFFT) or impulse response of the $H(\omega)$. Thus, the output of the system, $y(t)$, is given by the convolution of $h(t)$ with $u(t)$: $y(t) = h(t) * u(t)$. We estimated the output of the endogenous transfer function ($y(t)$) by taking the average of the 50 responses to $u(t)$ computed for each segment. Let g_1 and g_2 be the iFFT of G_1 and G_2, respectively. Then, let y_1 and y_2 be the outputs of systems g_1 and g_2, respectively. Thus, by analogy, $y_1(t) = g_1(t) * u(t)$ and $y_2(t) = g_2(t) * u(t)$. Once the responses to $u(t)$ were estimated, we matched the sampling rates and synchronized all outputs with the respective EPs using cross-correlation. First, we compared G_1 and G_2 responses (y_1 and y_2) with the direct EP, in order to confirm which one better replicates the EP. Then, we computed the fraction of variance explained in $y_1(t)$ and $y_2(t)$ by the average response of all 50 transfer functions computed from the endogenous signals ($y(t)$), R_1^2, and R_2^2, respectively. This allowed us to verify whether the estimated transfer function from endogenous data ($H(\omega)$) estimates the direct EP.

Finally, We fitted a regression line to each pair of DBS EPs and estimated responses of $H(\omega)$ to compute R^2. We computed ∼50 repeated measures of R^2s for each pathway and each direction per subject. Among these 50 predictions, we marked the ones that were greater than 3 strandard deviation from the mean as outliers (limiting to a maximum of 5 outliers for every 50 segments). Once the outliers were removed, a linear mixed effect model with repeated measure was employed using lme4 [26] packages in R-studio (R core team, 2021), with

the distant targets as the fixed effect and random intercepts for all subjects. Thereafter, we performed a multiple comparison using the emmeans [27] package to find the differences between each pathway (GPi-Vo, GPi-VA, and GPi-STN) and to discover which pathway response is more likely to be predicted by a linear transfer function representation of that pathway. We adjusted the p-values using Bonferroni correction. We performed the analysis with outliers included and outliers removed to confirm that the removal of outliers have not, significantly, affected the final results.

3 Results

For all subjects and all regions, the results showed that y_1 is highly correlated ($R^2 = 0.99$) with the actual recorded EP; thus provide evidence that the stimulation itself is more likely to cause the EP at the distant target, perhaps by direct excitation of efferent axons near the stimulation site, as opposed to an indirect response due to local excitation. In other words, the EP at the distance site is likely a direct result of the stimulation, rather than a result of excitation of neurons cell bodies near the stimulation site with subsequent propagation to the target. Therefore, for the remainder of this paper, "direct EP" will be referred to as y_1.

The results from comparison of $y(t)$, $y_1(t)$, and $y_2(t)$ for one subject are shown in Figure 5. As illustrated, R_1^2 (the fraction of variance explained in EP or $y_1(t)$ by $y(t)$) is significantly higher than R_2^2 (the fraction of variance explained in EP by $y(t)$). This result was consistent among all subjects and pathways (GPi-VO, GPi-VA, and GPi-STN), supporting that the ETFE potentially predicts the direct effect of stimulation on the distant target, rather than predicting some other underlying neural transmission.

Next, in order to determine whether the DBS pulses are reaching the distant targets through pathways similar to the endogenous signals or not, we tested the reliability and accuracy of the ETFE impulse responses and compared the predictions for all three pathways in both directions (forward and backward). In order to do so, we only compared our predictions with the $y_1(t)$ (direct EP) for each pathway in each direction by computing the fraction of variance explained in $y_1(t)$ by $y(t)$. We used the linear mixed effect model fitted to the R_1^2 (fraction of variance explained in $y_1(t)$ by $y(t)$) to compare the quality of prediction in all three pathways, forward and backward. The model coefficient of determination (R^2) was 0.25. The results of multiple comparison between the pathways shown in Figure 6, demonstrate that the predicted system outputs have stronger correlation with the DBS EPs in VO and STN compared to the DBS EPs in VA ($p - value \prec .01$). The high fraction of variance of EP explained by the output of the transfer function H $(y(t))$ reveals that the pathways that transmit external electrical stimulation mostly include pathways that transmit endogenous neural signals (GPi to VO and GPi to STN). In other words, the pathways that transmit external electrical stimulation overlap with the pathways that transmit endogenous neural signals such as GPi-VO, and this method can be used to

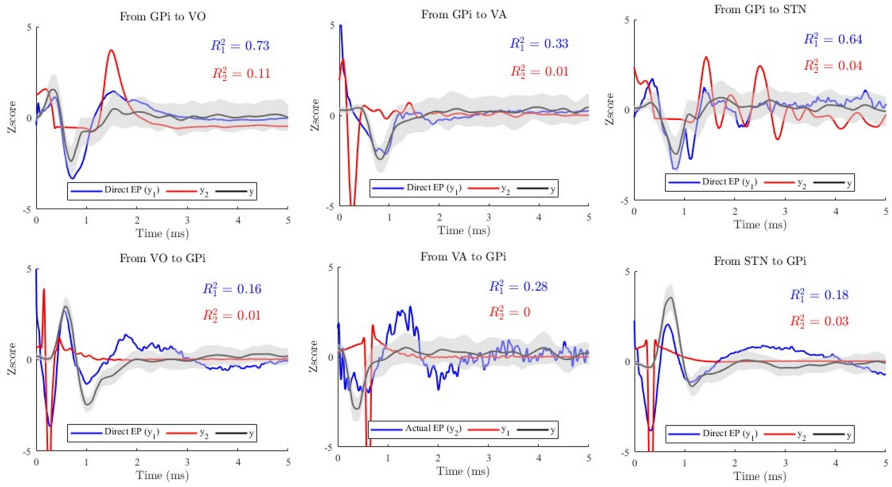

Fig. 5: The figures show the true responses in VO, VA, and STN, evoked by stimulation in GPi ($y_1(t)$, blue lines). They also illustrate the estimated output of the transfer function G_2 ($y_2(t)$, red lines) as well as the response of the endogenous data transfer function H ($y(t)$, black lines, averaged over ∼50 segments) and its standard deviation with 95% confidence interval (gray shade). In all cases, the impulse response of the ETFE explains a high variance of direct EP or $y_1(t)$, and not the $y_2(t)$.

potentially predict the DBS transmission through the brain network. Furthermore, we were able to predict the VA, VO, and STN responses to simulation in GPi significantly better than the GPi response to stimulation in VA, VO, and STN ($p - value \prec .01$), respectively. This observation may be explained by underlying anatomical and physiological differences in the fibers connecting two targets (fiber size, anisotropy, and diffusivity or direction of endogenous signal transmission; orthodromic versus antidromic).

4 Discussion

In this study, we provided evidence that it may be possible to estimate the causal flow of endogenous signals by comparing DBS EPs (which indicate causal flow of exogenous signals) with an empirical transfer function (ETFE) response derived from endogenous signals (which only indicates correlation). Since we stimulated in GPi and recorded in thalamus and STN, it is reasonable to expect that external evoked responses were primarily carried by orthodromic pathways. We additionally included GPi responses to the thalamic nuclei and STN stimulation in our analyses to compare the ETFE prediction accuracy in one direction versus the opposite direction. This allowed us to conclude that the ETFEs are a good estimate of direction of pathways in GPi to thalamic subnuclei (VO and VA)

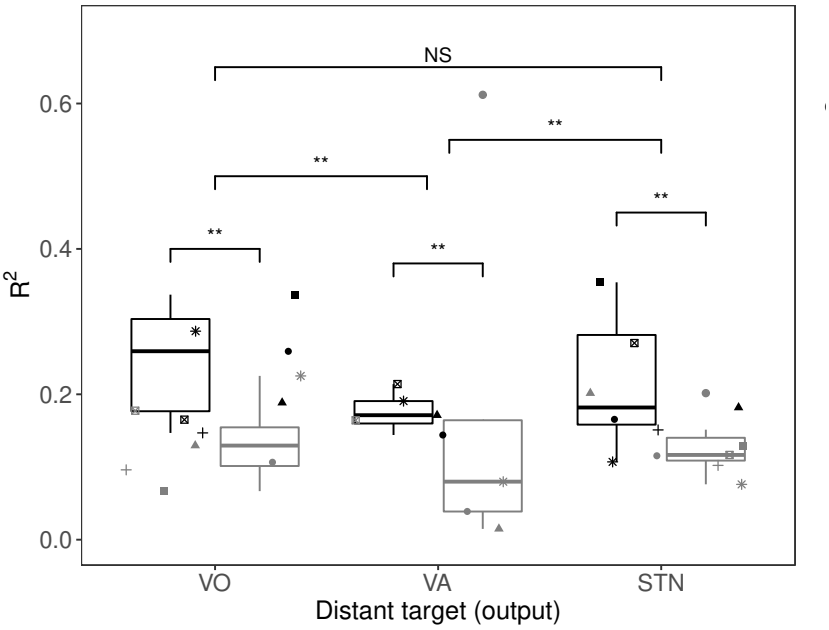

Fig. 6: The fraction of variance (R^2) of DBS EP explained by the endogenous transfer functions of each pathway (black: pathways from GPi; gray: pathways to GPi) for the seven subjects (each shape represents one subject). The variance explained is greater for STN and Vo ($p{-}value \prec .01$) compared to VA, suggesting that the exogenous signals from GPi to STN and Vo are more likely to use the same pathways as endogenous signals, compared to the GPi-VA pathway between the electrode locations. However, the fraction of variance explained in EP by the intrinsic transfer functions of GPi-VO and GPi-STN are not significantly different from each other. Moreover, the results also demonstrate that the ETFEs were able to make better predictions of EP in one direction (from GPi to other targets) compared to the reverse direction (from other nuclei to GPi) ($p{-}value \prec .01$).

projections; orthodromic versus antidromic. The higher correlations of ETFE responses with the thalamic DBS EPs in orthodromic (GPi to VA or Vo) versus antidromic (Vo or VA to GPi) pathways suggest that the higher fraction of DBS (exogenous signals) travel orthodromically (downstream) rather than antidromically. However, the higher correlation of GPi-STN impulse responses with the EP versus that of STN-GPi does not reflect the bidirectional connectivity between GPi and STN. On the other hand, higher correlation of the ETFE responses in GPi-VO, and GPi-STN, (in both directions) with the EPs compared to GPi-VA suggests that there are possibly fewer projections or fibers connecting two nuclei, leading to less flow of endogenous signals.

A potential limitation of this study is that subjects were performing voluntary movement during the recording of intrinsic brain activity, whereas they were at rest during the recording of electrical evoked responses. This element of study design was intentional, in order to evaluate whether signals associated with voluntary (but potentially abnormal) movement flow along the same pathways as DBS responses and whether connectivity in the resting state determines signal flow in the active state. Since we assume that a higher flow of movement-related information in the motor pathways could lead to stronger correlation between two ends of a motor pathway and therefore the obtained transfer function from the endogenous signal is a better representation of that pathway. Moreover, using this method ensures that the correlation between the ETFE predictions and the evoked potential are not related to voluntary movements.

In conclusion, our novel method provided strong evidence that (1) the neural responses to external stimulation are predictable and these responses are results of direct transmission on stimulation pulses to the distant target and (2) the proposed transfer function estimation approach has the potential to successfully predict DBS signal transmission, and possibly the causal direction of endogenous signals, for a known connection. These results infer that electrical stimulation in GPi travels at least in part along pathways that are part of the usual communication between GPi-VO and GPi-STN, and to a lesser extent between GPi-VA. These findings build on what is already established regarding GPi projections to the thalamus nuclei, VO and VA within the motor pathway circuit. The transfer function presented here enables us to make predictions about the effect of stimulation based on intrinsic signals collected during movement in the absence of stimulation, suggesting that the off-stim oscillations dynamics contain useful information about the network responses to DBS pulses. Our method suggests a number of areas for further research and promises to inform the development of novel techniques for the study of DBS.

In future research, we plan to determine if there are notable differences between anatomical and non-anatomical pathways by analyzing recordings from a larger patient population. We also intend to use this approach to study the impact of DBS on deep brain network activity in the frequency domain and find the relationship of these transfer function gains with anatomical connections derived from tractography.

Acknowledgements. We thank our volunteers and their parents for participating in this study. We also thank Jennifer MacLean for her assistance with neurologic examinations, as well as Jaya Nataraj for helping in data collection. This study is funded by the Cerebral Palsy Alliance Research Foundation (PG02518).

Conflicts of Interest. All authors declare no conflicts of interest.

References

[1] Terence D. Sanger. "Deep brain stimulation for cerebral palsy: where are we now?" In: *Developmental Medicine and Child Neurology* 62.1 (2020), pp. 28–33. ISSN: 14698749. DOI: 10.1111/dmcn.14295.

[2] Terence D Sanger et al. "Case Report: Targeting for Deep Brain Stimulation Surgery Using Chronic Recording and Stimulation in an Inpatient Neuromodulation Monitoring Unit, With Implantation of Electrodes in GPi and Vim in a 7-Year-Old Child With Progressive Generalized Dystonia." eng. In: *Journal of child neurology* 33.12 (2018), pp. 776–783. ISSN: 1708-8283 (Electronic). DOI: 10.1177/0883073818787741.

[3] Terence D et al. Sanger. "Pediatric Deep Brain Stimulation Using Awake Recording and Stimulation for Target Selection in an Inpatient Neuromodulation Monitoring Unit." eng. In: *Brain sciences* 8.7 (2018). ISSN: 2076-3425 (Print). DOI: 10.3390/brainsci8070135.

[4] Maral Kasiri et al. "Correlated activity in globus pallidus and thalamus during voluntary reaching movement in three children with primary dystonia". In: *Dystonia* 2 (2023). ISSN: 2813-2106. DOI: 10.3389/dyst.2023.11117. URL: https://www.frontierspartnerships.org/articles/10.3389/dyst.2023.11117.

[5] Ellen L. Air et al. "Deep brain stimulation in children: Experience and technical pearls. Clinical article". In: *Journal of Neurosurgery: Pediatrics* 8.6 (2011), pp. 566–574. ISSN: 19330707. DOI: 10.3171/2011.8.PEDS11153.

[6] Satomi Chiken and Atsushi Nambu. *Disrupting neuronal transmission: Mechanism of DBS?* 2014. DOI: 10.3389/fnsys.2014.00033.

[7] Terence D Sanger. "A Computational Model of Deep-Brain Stimulation for Acquired Dystonia in Children". In: *Frontiers in Computational Neuroscience* 12 (2018). ISSN: 1662-5188. DOI: 10.3389/fncom.2018.00077.

[8] David A Peterson, Terrence J Sejnowski, and Howard Poizner. "Convergent evidence for abnormal striatal synaptic plasticity in dystonia". In: *Neurobiology of Disease* 37.3 (2010), pp. 558–573. ISSN: 0969-9961. DOI: 10.1016/j.nbd.2009.12.003.

[9] Yanan et al. Sui. "Deep Brain Stimulation Initiative: Toward Innovative Technology, New Disease Indications, and Approaches to Current and Future Clinical Challenges in Neuromodulation Therapy". In: *Frontiers in Neurology* 11 (2021). ISSN: 1664-2295. DOI: 10.3389/fneur.2020.597451.

[10] Cameron C McIntyre and Thomas J Foutz. "Computational modeling of deep brain stimulation." eng. In: *Handbook of clinical neurology* 116 (2013), pp. 55–61. ISSN: 0072-9752 (Print). DOI: 10.1016/B978-0-444-53497-2.00005-X.

[11] Bruce Luber et al. "Using diffusion tensor imaging to effectively target TMS to deep brain structures". In: *NeuroImage* 249 (2022), p. 118863. ISSN: 1053-8119. DOI: 10.1016/j.neuroimage.2021.118863.

[12] Cynthia R Steinhardt et al. "Characterizing and predicting cortical evoked responses to direct electrical stimulation of the human brain". In: *Brain Stimulation* 13.5 (2020), pp. 1218–1225. ISSN: 18764754. DOI: 10.1016/j.brs.2020.05.001.

[13] Chi-Tsong Chen. *Linear System Theory and Design*. 3rd. USA: Oxford University Press, Inc., 1998. ISBN: 0195117778.

[14] R A González et al. "Optimal Enforcement of Causality in Non-Parametric Transfer Function Estimation". In: *IEEE Control Systems Letters* 1.2 (2017), pp. 268–273. ISSN: 2475-1456 VO - 1. DOI: 10.1109/LCSYS.2017.2713821.

[15] José L Lanciego, Natasha Luquin, and José A Obeso. "Functional neuroanatomy of the basal ganglia". eng. In: *Cold Spring Harbor perspectives in medicine* 2.12 (2012), a009621–a009621. ISSN: 2157-1422. DOI: 10.1101/cshperspect.a009621.

[16] Jessica S L Vidmark, Estefania Hernandez-Martin, and Terence D Sanger. "Increasing Consistency of Evoked Response in Thalamic Nuclei During Repetitive Burst Stimulation of Peripheral Nerve in Humans". In: *Lecture Notes in Computer Science*. Ed. by Marleen de Bruijne et al. Cham: Springer International Publishing, 2021, pp. 238–247. ISBN: 978-3-030-87237-3.

[17] Terence Sanger et al. "Classification and Definition of Disorders Causing Hypertonia in Childhood". In: *Pediatrics* 111 (Apr. 2003), e89–97. DOI: 10.1542/peds.111.1.e89.

[18] Lucia Abela and Manju Ann Kurian. *KMT2B-Related Dystonia Synonyms: DYT28, DYT-KMT2B*. 1993. URL: https://www.ncbi.nlm.nih.gov/books/.

[19] Estefania Hernandez-Martin et al. "Evoked Potentials During Peripheral Stimulation Confirm Electrode Location in Thalamic Subnuclei in Children With Secondary Dystonia". In: *Journal of Child Neurology* 35 (12 2020). PMID: 32567481, pp. 799–807. DOI: 10.1177/0883073820931970. URL: https://doi.org/10.1177/0883073820931970.

[20] Estefania Hernandez-Martin et al. "Globus pallidus internus activity increases during voluntary movement in children with dystonia". In: *iScience* 26 (June 2023). DOI: 10.1016/j.isci.2023.107066. URL: https://www.sciencedirect.com/science/article/pii/S2589004223011434.

[21] Vasilis Marmarelis. *Analysis of physiological systems: The white-noise approach*. Springer Science & Business Media, 2012.

[22] Nicholas C Sinclair et al. "On the neural basis of deep brain stimulation evoked resonant activity". In: *Biomedical Physics & Engineering Express*

5 (5 Aug. 2019), p. 57001. DOI: 10.1088/2057-1976/ab366e. URL: https://dx.doi.org/10.1088/2057-1976/ab366e.

[23] Bowman, Adrian W. and Adelchi Azzalini. *Applied Smoothing Techniques for Data Analysis*. English. 1997.

[24] William S Cleveland. "Robust locally weighted regression and smoothing scatterplots". In: *Journal of the American Statistical Association* 74.368 (1979), pp. 829–836. ISSN: 1537274X. DOI: 10.1080/01621459.1979.10481038.

[25] Anders Stenman et al. "On adaptive smoothing of empirical transfer function estimates". In: *Control Engineering Practice* 8.11 (2000), pp. 1309–1315. ISSN: 0967-0661. DOI: 10.1016/S0967-0661(00)00065-4.

[26] Douglas Bates et al. "Fitting Linear Mixed-Effects Models Using lme4". In: *Journal of Statistical Software* 67 (1 2015), pp. 1–48. DOI: 10.18637/jss.v067.i01. URL: https://www.jstatsoft.org/index.php/jss/article/view/v067i01.

[27] S R Searle, F M Speed, and G A Milliken. "Population Marginal Means in the Linear Model: An Alternative to Least Squares Means". In: *The American Statistician* 34 (4 1980), pp. 216–221. DOI: 10.1080/00031305.1980.10483031. URL: https://www.tandfonline.com/doi/abs/10.1080/00031305.1980.10483031.